Fade Mitigation Based on Semiconductor Optical Amplifiers

Konstantinos Yiannopoulos, *Member, IEEE*, Nikos C. Sagias, *Senior Member, IEEE*, and Anthony C. Boucouvalas, *Fellow, IEEE*

***Abstract*—We present and analyze a novel fade mitigation technique that is applicable on outdoor optical wireless systems. Our key idea is to utilize the nonlinear power-dependent gain properties of a semiconductor optical amplifier (SOA) to provide unbalanced amplification between faded and non-faded instances of the optical wireless signal. We analytically demonstrate that this power equalization process smoothes out fade-induced power fluctuations and drastically reduces the probability of the system being in a fade state. In medium to strong turbulence governed by gamma-gamma statistics, our results predict that the fade probability can be reduced by over 80% when the SOA is introduced at the optical wireless receiver. We also show that the duration of remaining fades is reduced by a sizeable percentage, and a percentile reduction of the average fade duration of over 85% can be achieved at the SOA output.**

***Index Terms*—Average fade duration, gamma-gamma fading, level crossing rates (LCR), outdoor optical wireless, scintillation index (SI), semiconductor optical amplifier (SOA).**

I. Introduction

OUTDOOR optical wireless (OW) systems have recently gained attention as a broadband alternative in niche applications including semi-permanent office interconnections and MAN implementations [1]. While outdoor OW may not directly compete with WDM fiber networks in terms of total capacity, contemporary commercial systems are well capable of providing 10 Gb/s speeds and even higher speeds are expected in the future. Moreover, outdoor OW is cost-effective in terms of deployment, since the link can be installed without digging/repairing roads, while no special spectrum license fees are required. OW systems it can also be deployed in a plug-and-play manner for providing extra capacity over installed fiber links whenever required.

Despite the inherent advantages of outdoor OW systems, the transmission of light through the atmosphere can be challenging [2]–[4]. Apart from weather-dependent static transmission losses that may limit the system availability, atmospheric turbulence induces time-varying changes in the refractive index, which in turn affect the amplitude, phase and propagation direction of the optical signal. These changes result in time-varying power fluctuations of the received signal and when the turbulence is intense enough, the received signal decreases below the receiver sensitivity and the link is lost. This corresponds to a fade event, which affects the OW system both in terms of capacity, as well as latency. Several million bits may be lost during a msec-long fade at 10 Gb/s, while the link will be in outage for an amount of time approximately equal to the fade duration.

Mitigating fades is, thus, of significant importance for optimizing the operation of the OW system and a number of techniques have been proposed for decreasing the fade duration and minimizing their impact on the system performance. In weak (log-normal) fading conditions, it is sufficient to utilize an aperture-averaging technique, where a large-aperture receiver collects stray light [5]. The mitigation of more intense fading, however, requires techniques that incorporate some form of diversity, either spatial or temporal. Spatial diversity [6]–[10] utilizes multiple links between the transmitter(s) and the receiver(s), aiming to de-correlate the operation of individual links, so that fading does not affect all links simultaneously. This is accomplished by adjusting the lateral distance between links to exceed the correlation length of the atmosphere. Temporal diversity, on the other hand, utilizes time-delayed replicas of the transmitted signal [11], [12]. The temporal delay between replicas is designed to exceed the expected fade duration, and as a result, at least one of the replicas is not affected by the fade and is successfully received. More advanced mitigation techniques can be implemented using the aforementioned schemes in conjunction with sophisticated coding schemes [12]–[15], for example rate-less coding, which essentially adjust the transmission rate so as to match the channel capacity at any given time [16].

In the current study, we analyze an alternative technique for fade mitigation that involves optical signal equalization in semiconductor optical amplifiers (SOAs) [17]. In the proposed technique, the SOA provides unbalanced gain to the incoming OW signal, depending on the fade conditions. If the link is in a fade state, then the SOA is not saturated by the OW signal and provides maximum gain. On the other hand, the OW signal fully saturates the SOA at the absence of fades and experiences limited or no gain at all. We demonstrate that this unbalanced operation of the SOA a) reduces the power fluctuations of the incoming signal, and thus, limits the probability of the system being in a fade condition, while b) remaining fades exhibit significantly decreased duration. In addition, we discuss the optimal operational conditions that correspond to minimizing the probability

Manuscript received July 19, 2013; revised September 13, 2013; accepted October 3, 2013. Date of publication October 8, 2013; date of current version November 6, 2013. This work was supported by the University of Peloponnese internal project FAMOOSE and by COST Action IC1101 "Optical Wireless Communications—An Emerging Technology." This paper was submitted in part at the IEEE Wireless Communications and Networking Conference, Istanbul, Turkey, April 6–9, 2014.

The authors are with the Department of Informatics and Telecommunications, University of Peloponnese, 22100 Tripoli, Greece (e- mail: kyianno@uop.gr; nsagias@ieee.org; acb@uop.gr).

Digital Object Identifier 10.1109/JLT.2013.2285260

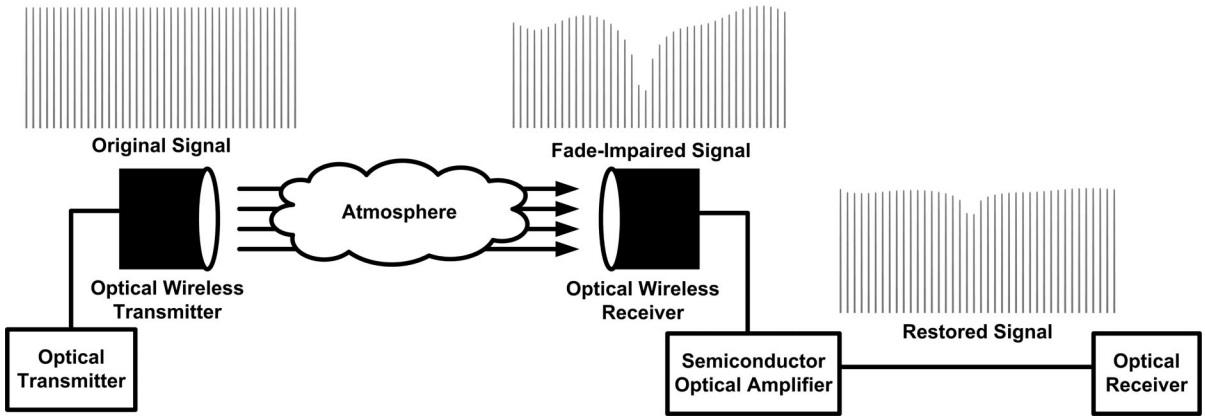

Fig. 1. Principle of operation of the proposed technique.

of fades and their duration, and show that a) high small signal gain SOAs are preferable, and b) there is no real benefit from raising the average received signal power over 70% of the SOA saturation power.

The rest of this paper is organized as follows. In Section II we elaborate on the principle of operation of the proposed technique and analytically derive the probability density function of fades at the SOA output. In Section III, we discuss the performance enhancement that is achieved by utilizing the SOA in terms of reducing the fade probability. We also determine in an analytical fashion the SOA attributes (small signal gain and saturation power) that correspond to optimal operation. In Section IV we calculate the average fade duration (AFD) at the SOA output and demonstrate that it is drastically reduced when the system operation complies with the operational conditions determined earlier. Finally, concluding remarks are given in Section V.

II. Proposed System Model

The proposed system setup and its operation are summarized in Fig. 1. We consider a $\lambda = 1550$ nm OW link that is used to communicate optical pulses between two remote stations through the atmosphere, and atmospheric effects (turbulence) attenuate the power levels of optical pulses in a stochastic manner. As a result, the received signal exhibits random power fluctuations (fades), whose intensity and duration are dictated by the turbulence statistics. In order to alleviate the fades induced by the OW channel and restore the original signal prior to reception, a SOA is employed at the output of the optical antenna and before the receiver photodiode. The SOA serves as a 2R regenerator based on the self-gain modulation (SGM) effect, which provides increasing gain to optical pulses as their power levels diminish.

A. SOA Time Domain Analysis

To better illustrate the principle of SGM-based regeneration in the presence of fades, we consider the analytical SOA gain noiseless model presented in [18], [19]. Following the analysis found therein, an optical pulse that enters the SOA saturates its gain and the instantaneous gain response at time t is given by

$$G(t) = \left[1 - \left(1 - \frac{1}{G_0}\right) \exp\left(-\frac{U_{\rm in}(t)}{U_{\rm sat}}\right)\right]^{-1} \quad (1)$$

where $U_{\rm sat}$ is the saturation energy of the SOA and G_0 is its small signal gain. $U_{\rm in}(t)$ corresponds to the temporal profile of the input pulse energy that is calculated from the instantaneous pulse power $P_{\rm in}(t)$ as

$$U_{\rm in}(t) = \int_0^t P_{\rm in}(\tau)\, d\tau. \quad (2)$$

The temporal profile of the output pulse energy $U_{\rm out}(t)$ is obtained from (1) and (2), and it can be shown that it is related to the input energy profile as [18], [19]

$$\begin{aligned} U_{\rm out}(t) &= \int_0^t G(\tau)\, P_{\rm in}(\tau)\, d\tau \\ &= U_{\rm sat}\, \log\left[1 + G_0\, \left(\exp\left(\frac{U_{\rm in}(t)}{U_{\rm sat}}\right) - 1\right)\right]. \end{aligned} \quad (3)$$

Equation (3) summarizes the instantaneous equalization properties of the SOA. It is straightforward to verify that when the SOA is operated at low input energies, then its response is almost linear and the instantaneous energy gain equals G_0. On the other hand, high input powers heavily saturate the SOA and the instantaneous energy gain can be approximated by $\log(G_0)$. The energy-dependent SOA operation serves to equalize pulse energies and this attribute can be utilized to mitigate fades in an OW environment. Optical pulses that have not experienced intense fading over the OW channel will maintain adequate energy to saturate the SOA and will receive limited gain, according to (3). On the other hand, fade-impaired pulses will experience a significantly higher gain (ideally up to G_0), since their energy is much lower than the saturation energy of the SOA.

We further demonstrate the power equalization capabilities of the proposed technique in an analytical fashion by calculating the probability density function (pdf) of the signal envelope at the output of the SOA. To this end, we assume that the transmitted optical signal comprises a series of short return-to-zero (RZ) optical pulses at a bit period of T_b

$$P_{\rm Tx}(t) = P_0 \sum_{n=-\infty}^{\infty} p\,(t - n\,T_b) \quad (4)$$

with $p(t)$ being the temporal pulse profile, and that individual pulses have a unity average power

$$\frac{1}{T_b}\int_0^{T_b} p(t)\,dt = 1 \tag{5}$$

so that the average signal power at the transmitter equals P_0. The transmitted optical signal is distorted by turbulence in the OW channel and the instantaneous received signal power can be expressed as

$$P_{\rm Rx}(t) = P_{\rm ch}(t)\sum_{n=-\infty}^{\infty} p\left(t - n\,T_b\right) \tag{6}$$

where $P_{\rm ch}(t)$ is the stochastic optical channel response. Channel variations typically occur at μsec scales (or longer), while bit durations are limited to hundreds of psec for the line rates under consideration, and as a result the channel response can be considered a slowly varying envelope that modulates the amplitudes of the received pulses but not their temporal profile. The instantaneous power of each received pulse is then expressed as

$$P_{\rm in}(\tau) = P_{\rm ch}\left(n\,T_b\right)\,p(\tau), \quad 0 \le \tau < T_b. \tag{7}$$

B. Channel Model

Various statistical models have been proposed in order to describe the optical channel characteristics with respect to the atmospheric turbulence strength. It has been observed that for moderate-to-strong fluctuations, the distribution of the received intensity is close to gamma-gamma ($\gamma-\gamma$) [20], resulting as a multiplication of two independent Gamma random processes. The $\gamma-\gamma$ distribution is used to model both small- and large-scale fluctuations and provides good agreement between theoretical and experimental data. Following (7), the average power $P_{\rm in}$ of each pulse obeys the same statistics with the channel response having $\gamma-\gamma$ pdf given by [21, (2)]

$$f_{P_{\rm in}}(z) = \frac{2\,\left(m_y\,m_x\right)^{\frac{m_y+m_x}{2}}}{\Gamma\left(m_x\right)\,\Gamma\left(m_y\right)}\,\frac{z^{\frac{m_y+m_x}{2}-1}}{\overline{P}_{\rm in}^{\frac{m_y+m_x}{2}}} \times K_{m_y-m_x}\left(2\sqrt{m_y\,m_x\,\frac{z}{\overline{P}_{\rm in}}}\right). \tag{8}$$

In (8), $\overline{P}_{\rm in}$ is the average received optical power, while $\Gamma(\cdot)$ and $K_v(\cdot)$ denote the Gamma and second kind modified Bessel functions, respectively. Moreover, m_x and m_y are two $\gamma-\gamma$ distribution parameters related to the effective numbers of large- and small-scale scatterers in the OW link. More details about the $\gamma-\gamma$ model parameters are given in the Appendix.

C. SOA Output Statistics

The received optical pulses traverse the SOA and each one experiences a gain that is dependent on its energy, as it has been detailed previously. Assuming that the gain recovery time is limited to less than one bit period, so that the device fully recovers to G_0 after each incoming pulse, we utilize (3) to correlate input and output pulse energies from the corresponding temporal profiles as

$$U_{\rm out} = U_{\rm sat}\,\log\left[1 + G_0\left(\exp\left(\frac{U_{\rm in}}{U_{\rm sat}}\right) - 1\right)\right]. \tag{9}$$

Since pulse energies are proportionally related to average optical powers as

$$U_{\rm in} = P_{\rm in}\,T_b \tag{10a}$$

and

$$U_{\rm out} = P_{\rm out}\,T_b \tag{10b}$$

equation (9) can be rewritten as

$$\exp\left(\frac{P_{\rm out}}{P_{\rm sat}}\right) - 1 = G_0\left[\exp\left(\frac{P_{\rm in}}{P_{\rm sat}}\right) - 1\right] \tag{11}$$

with $P_{\rm sat}$ being the rate-dependent saturation parameter of the SOA

$$P_{\rm sat} = \frac{U_{\rm sat}}{T_b}. \tag{12}$$

By applying the transformation of variables given by (11) to the $\gamma-\gamma$ pdf of (8), the pdf of the optical signal envelope at the output of the SOA can be obtained as

$$f_{P_{\rm out}}(z) = \frac{2}{G_0}\,\frac{\left(m_y\cdot m_x\right)^{\frac{m_y+m_x}{2}}}{\Gamma\left(m_y\right)\cdot\Gamma\left(m_x\right)}\,\frac{\exp\left(z/P_{\rm sat}\right)}{\mathcal{T}\left(z/P_{\rm sat}\right)} \times \frac{P_{\rm sat}^{\frac{m_y+m_x}{2}-1}}{\overline{P}_{\rm in}^{\frac{m_y+m_x}{2}}}\,\left[\log\left(\mathcal{T}\left(\frac{z}{P_{\rm sat}}\right)\right)\right]^{\frac{m_y+m_x}{2}-1} \times K_{m_y-m_x}\left(2\sqrt{m_y\,m_x\,\frac{P_{\rm sat}}{\overline{P}_{\rm in}}\cdot\log\left[\mathcal{T}\left(\frac{z}{P_{\rm sat}}\right)\right]}\right) \tag{13}$$

with $\mathcal{T}(x) = [G_0 - 1 + \exp(x)]/G_0$. For discussion purposes, we define the normalization parameters r (normalized input power) and u (normalized output power) as

$$r = \frac{\overline{P}_{\rm in}}{P_{\rm sat}} \tag{14a}$$

and

$$u = \frac{P_{\rm out}}{\overline{P}_{\rm in}} \tag{14b}$$

respectively, to obtain the normalized SOA output power pdf

$$f_u(z) = \frac{2}{G_0}\,\frac{\left(m_y\,m_x\right)^{\frac{m_y+m_x}{2}}}{\Gamma\left(m_x\right)\,\Gamma\left(m_y\right)}\,\frac{\exp(r\,z)}{\mathcal{T}(r\,z)} \times r^{1-\frac{m_y+m_x}{2}}\,\left[\log\left(\mathcal{T}(r\,z)\right)\right]^{\frac{m_y+m_x}{2}-1} \times K_{m_y-m_x}\left[2\sqrt{\frac{m_y\,m_x}{r}\,\log\left(\mathcal{T}(r\,z)\right)}\right]. \tag{15}$$

Equation (15) is plotted in Figs. 2 and 3 for a 500 m OW link with parameters that are summarized in Tables I and II. Both figures show that the pdf at the SOA output varies significantly from the original $\gamma-\gamma$, and exhibits a strong peak that owes to the power equalization process in the SOA. The peak clearly

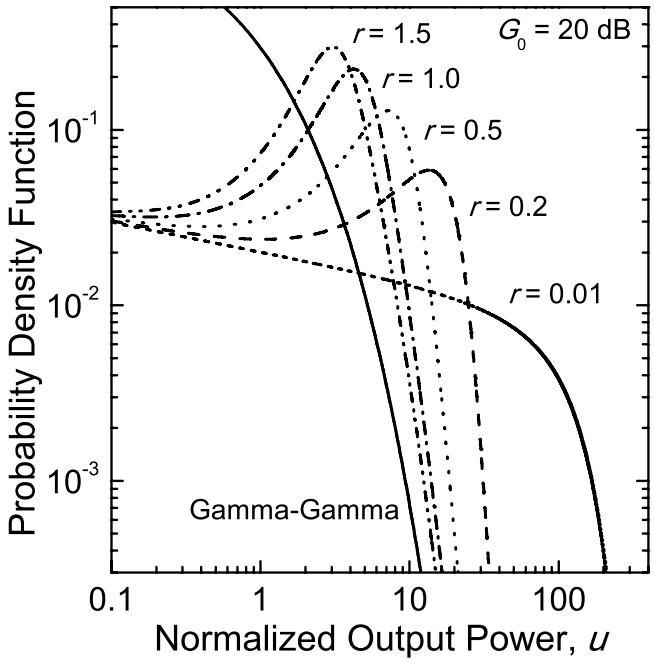

Fig. 2. Probability density function of the SOA normalized optical output power versus the normalized output power for $G_0 = 20$ dB.

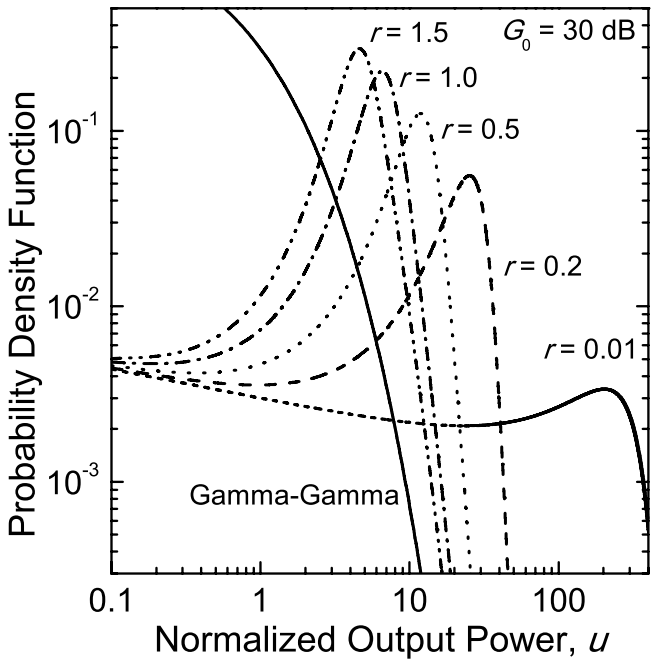

Fig. 3. Probability density functions of the SOA normalized optical output power versus the normalized output power for $G_0 = 30$ dB.

TABLE I
OPTICAL WIRELESS LINK PARAMETERS

Parameter	Symbol	Value
Refractive index structure	C_n^2	4.58×10^{-13} m$^{-2/3}$
Wavelength	λ	1550 nm
Mean traverse wind speed	v_T	1 m/sec
Receiver aperture diameter	D	10 mm
SOA gain	G_0	20 and 30 dB
Normalized input power	r	0.2, 0.5, 1.0, 1.5
Link length	L	500, 1000, 1500 m

TABLE II
GAMMA-GAMMA PARAMETERS

L (m)	m_x	m_y	$\sigma_{\gamma-\gamma}$	b_x	b_y
500	4.20	0.83	1.31	11.56	42.83
1000	5.54	0.39	1.79	3.93	48.46
1500	7.26	0.23	2.26	1.85	48.04

indicates that the output signal envelope concentrates around a fixed power level, determined mainly by the normalized input power r. When the average input power is low, then the pdf peak shifts to a higher normalized output power, due to the fact that the SOA provides more static gain in average. Sufficiently small input powers (r approaches zero) correspond to a state where the SOA is never saturated and always amplifies pulses by its small signal gain G_0. In this regime the SOA acts like a linear amplifier and the pdf of optical powers at its output is also $\gamma - \gamma$ with an average power equal to $G_0\,\overline{P}_{\rm in}$. On the other hand, increased input powers result to a shift of the pdf peak towards lower normalized output powers, since the SOA gain is deeply saturated by most pulses and provides low gain. If the input power is further increased (r tends to infinity), then the output pdf will revert to the original $\gamma - \gamma$, since every single pulse fully saturates the SOA and no equalization is feasible. Finally, the figures also suggest that the SOA small signal gain G_0 does not play an equally significant role in the equalization process and in the output pdf shape, but only serves to provide more gain in average. This is expected from the equalization process in the SOA, since the gain saturation is relatively insensitive to G_0, according to (9).

The presented analysis shows that deploying the SOA is beneficial from a fade mitigation perspective, still the equalization benefit strongly depends on the operational conditions (input power) and SOA attributes (saturation parameter and gain). Operating the SOA at input optical powers that are significantly lower or higher than its saturation parameter $P_{\rm sat}$, leads to output statistics that are also $\gamma - \gamma$, thus there is no benefit in terms of equalization from deploying the device. It is therefore of interest to clarify the operational conditions that favor the deployment of SOAs as power equalizers under signal fading conditions and obtain results that correspond to optimized operation. We perform this evaluation task for both first and second order statistics in the following two sections.

III. FIRST ORDER PERFORMANCE CRITERIA

The preceding analysis provides a proof-of-principle for SGM-based fade equalization in SOAs, still it is of importance from a system designer perspective to be able to a) analytically predict the equalization gain, verifying that equalization is actually performed, and b) optimize the system operation, especially power in terms of power budget and SOA parameter selection, against fading conditions. We perform the former task by providing results for the fade probability of the signal at the SOA output, while the latter task is accomplished by evaluating the scintillation index of the signal at the SOA output.

$$\Pr\{u<u_\tau\} = \pi\,\csc[\pi\,(m_y-m_x)]\left[\frac{{}_1F_2\left(m_x;1+m_x,1-m_y+m_x;\frac{m_y\,m_x}{r}\,\log\left(\mathcal{T}(r\,u_\tau)\right)\right)}{\Gamma(m_y)\,\Gamma(1+m_x)\,\Gamma(1-m_y+m_x)}\left(\frac{m_y\,m_x}{r}\,\log\left(\mathcal{T}(r\,u_\tau)\right)\right)^{m_x}\right.$$
$$\left.+\left(\frac{m_y\,m_x}{r}\,\log\left(\mathcal{T}(r\,u_\tau)\right)\right)^{m_y}\frac{{}_1F_2\left(m_y;1+m_y,1-m_x+m_y;\frac{m_y\,m_x}{r}\,\log\left(\mathcal{T}(m_y\,u_\tau)\right)\right)}{\Gamma(m_x)\,\Gamma(1+m_y)\,\Gamma(1-m_x+m_y)}\right] \quad (16)$$

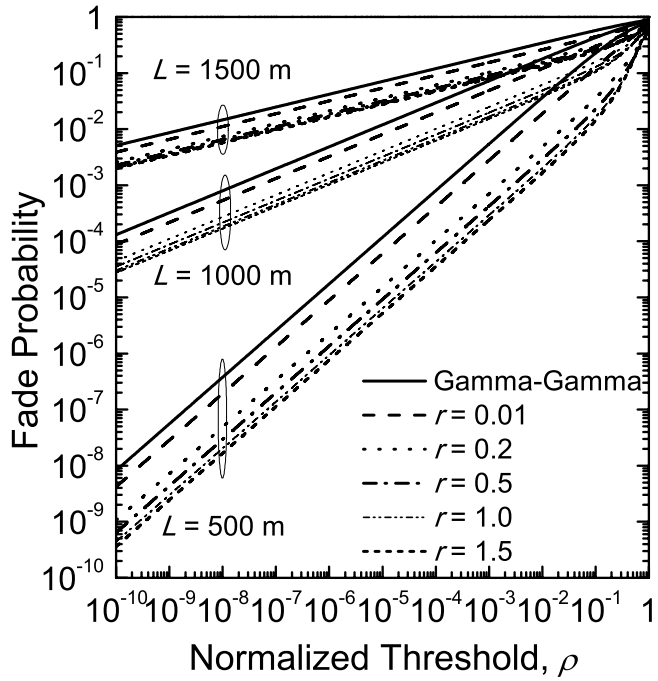

Fig. 4. Fade probability at the output of the SOA versus the normalized threshold ρ for SOA small signal gain $G_0 = 20$ dB.

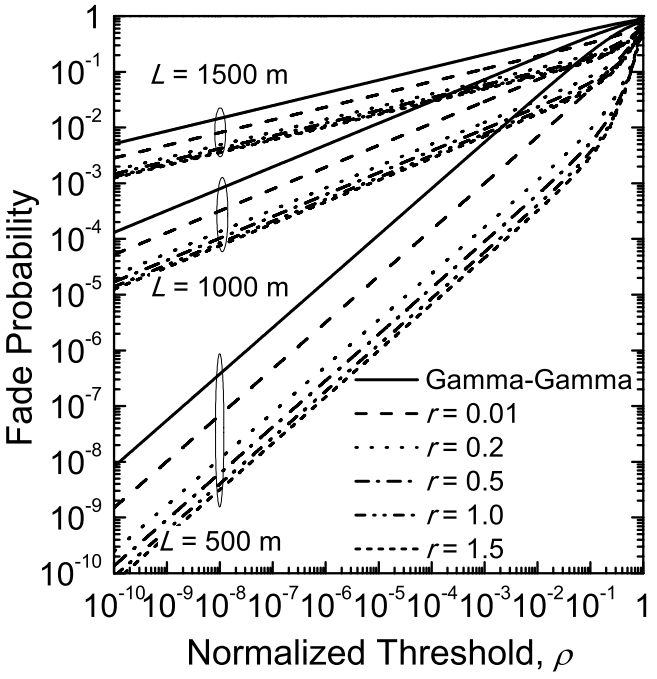

Fig. 5. Fade probability at the output of the SOA versus the normalized threshold ρ for SOA small signal gain $G_0 = 30$ dB.

A. Fade Probability

Let u_τ be a predetermined threshold, which is defined based on the bit-error probability (BER) requirements of the system. By considering that the normalized output power u remains below u_τ, the fade probability $\Pr\{u<u_\tau\} = \int_0^{u_\tau} f_u(z)\,dz$ can be obtained based on [22], [21, (3)] as in (16) (at the top of the next page), where ${}_pF_q(\cdot)$ is the generalized hypergeometric function, with p, q being integers.

Numerically evaluated fade probability curves are plotted in Figs. 4 and 5 against the receiver power threshold u_τ for three OW systems with links distances of $L = 500$, 1000 and 1500 m under moderate-to-strong turbulence scenarios [23]. The power threshold is normalized by the output power root-mean-square (rms) value $u_{\rm rms}$

$$\rho = \frac{u_\tau}{u_{\rm rms}} \quad (17)$$

which is numerically evaluated using

$$u_{\rm rms}^2 = \frac{2}{G_0}\,\frac{(m_y\cdot m_x)^{\frac{m_y+m_x}{2}}}{\Gamma(m_y)\,\Gamma(m_x)}\,r^{1-\frac{m_y+m_x}{2}}$$
$$\times\int_0^\infty \frac{z^2\,\exp(r\,z)}{\mathcal{T}(r\,z)}\,[\log(\mathcal{T}(r\,z))]^{\frac{m_y+m_x}{2}-1}$$
$$\times K_{m_y-m_x}\left[2\sqrt{\frac{m_y\,m_x}{r}\,\log\left(\mathcal{T}(r\,z)\right)}\right]dz. \quad (18)$$

for the parameters detailed in Tables I and II. This normalization is performed so as to take into account the average static gain which is provided by the SOA and affects the receiver power threshold for a given BER. The normalization also serves towards having a fair comparison between pdfs that correspond to different average output powers. Finally, we utilize the rms value of the output optical power instead of its mean value, considering that the optical signal is converted to electrical by a square-law detector (photodiode) at the receiver. Fig. 4 shows that the fade probability is considerably decreased when the SOA is deployed in comparison with the incoming $\gamma-\gamma$ signal. A fade probability decrease of over 87% is predicted for the 500 m link if a 20 dB small-signal gain SOA is utilized, while the same device attains a fade probability improvement of over 65% and 49% for the 1000 and 1500 m link, respectively. Even better results are obtained with a 30 dB gain SOA, and according to Fig. 5, the fade probability is reduced by 97%, 83% and 66% with increasing link distances. Moreover, the figure suggests that the attainable reduction saturates with the normalized input power, since powers of over 0.5 do not provide a noticeable decrease in the fade probability. As a result, operating the SOA

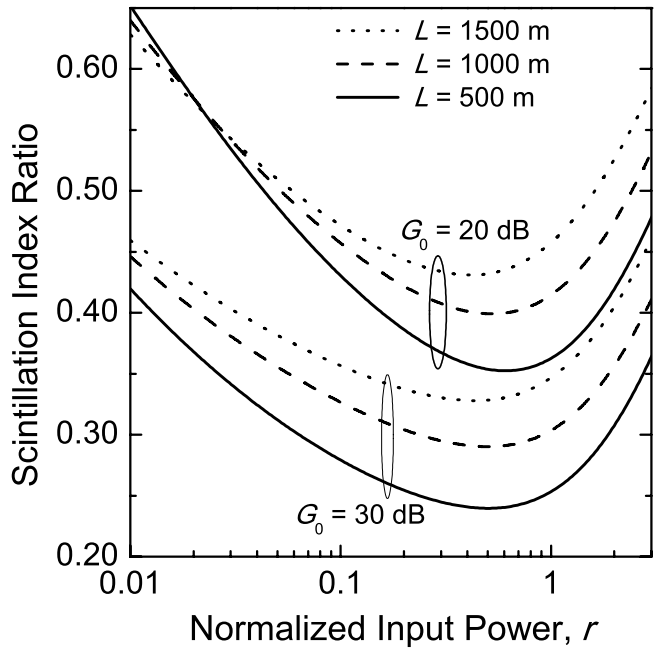

Fig. 6. Scintillation index ratio $\frac{\sigma_u}{\sigma_{\gamma-\gamma}}$ versus the normalized input power r.

at input powers over this value simply wastes energy over the OW link without providing an enhanced equalization benefit.

B. Scintillation Index

The last result of the previous subsection can be further explored using the scintillation index of the signal at the SOA output

$$\sigma_u = \frac{\sqrt{u_{\rm rms}^2 - \overline{u}^2}}{\overline{u}} \tag{19}$$

where

$$\overline{u} = \frac{2}{G_0} \frac{(m_y \cdot m_x)^{\frac{m_y+m_x}{2}}}{\Gamma(m_y)\cdot\Gamma(m_x)} r^{1-\frac{m_y+m_x}{2}} \times \int_0^\infty \frac{z\,\exp(r\,z)}{\mathcal{T}(r\,z)} \left[\log\left(\mathcal{T}(r\,z)\right)\right]^{\frac{m_y+m_x}{2}-1} \times K_{m_y-m_x}\left[2\sqrt{\frac{m_y\,m_x}{r}\,\log\left(\mathcal{T}(r\,z)\right)}\right] dz. \tag{20}$$

The scintillation index is associated with the amount of fading (AoF), which is a measure of the deviation of the signal around its mean value [24]. It is of interest to design the equalization system so that the scintillation index is minimized, since a close to zero value corresponds to an almost non-fluctuating signal.

The scintillation index is numerically evaluated from (19) and is plotted in Fig. 6 against the normalized input power, after being divided by the SOA input $(\gamma-\gamma)$ scintillation index

$$\sigma_{\gamma-\gamma} = \sqrt{\frac{1}{m_x} + \frac{1}{m_y} + \frac{1}{m_x\,m_y}} \tag{21}$$

so that a percentile rather than absolute reduction is illustrated. Fig. 6 clearly illustrates that the output signal scintillation index is significantly lower than that of the original $\gamma-\gamma$. A scintillation index decrease of 50%–65% can be observed for a 20 dB gain SOA, while a further 10% improvement can be obtained with a 30 dB gain SOA for all presented scenarios. As far as the input power is concerned, the scintillation index is minimized for input powers around 40%–70% of the saturation power irrespective of the fading intensity. This result is in close agreement to the input power requirements that were obtained via the fade probability analysis.

IV. Second Order Performance Criteria

The fade mitigation capabilities of the proposed setup are also demonstrated by the second order statistics of the signal at the output of the SOA. Even though the SOA drastically reduces the fade probability, as we have demonstrated in the previous section, fades are still expected to occur and it is of practical importance to have an estimation of the AFD. This is particularly true when trying to evaluate the OW system performance in terms of latency, since latency strongly depends on the AFD.

The AFD at the output of the SOA is calculated from the output signal level crossing rate (LCR), which in turn requires the knowledge of the joint pdf between the output signal and its time derivative. The joint pdf at the SOA output will be calculated from the joint pdf of the $\gamma-\gamma$ faded input signal that is given in integral form by [25]

$$f_{v,\dot{v}}(z,w) = \frac{1}{\sqrt{8\,\pi}} \frac{m_x^{m_x}\,m_y^{m_y}\,z^{m_y-\frac{3}{2}}}{\Gamma(m_x)\,\Gamma(m_y)} \int_0^\infty \frac{x^{m_x-m_y-\frac{1}{2}}}{\sqrt{b_x^2\,z + b_y^2\,x^2}} \times \exp\left[-m_x\,x - \frac{m_y z}{x} - \frac{w^2 x}{8z(b_x^2 z + b_y^2 x^2)}\right] dx. \tag{22}$$

Analytical relations for the calculation of parameters b_x and b_y, which correspond to the rapidity of fading due the large and small scale scattering, are given in the Appendix.

We utilize (11) to obtain the relations between the input and output signals and their time derivatives

$$v = \frac{1}{r}\,\log\left[\frac{G_0 - 1 + \exp(r\,u)}{G_0}\right] \tag{23a}$$

$$\dot{v} = \frac{\exp(r\,u)}{G_0 - 1 + \exp(r\,u)}\,\dot{u} \tag{23b}$$

and after applying the variable transform of (23) to (22), we find that the joint pdf at the SOA output equals to

$$f_{u,\dot{u}}(z,w) = \frac{\exp(2\,r\,z)}{G_0^2\,\mathcal{T}^2(r\,z)}\,f_{v,\dot{v}}\left(\frac{\log\left[\mathcal{T}(r\,z)\right]}{r}, \frac{w\,\exp(r\,z)}{G_0\,\mathcal{T}(r\,z)}\right). \tag{24}$$

Using the above equation and the definition of LCR, i.e. $\mathrm{LCR}(u_\tau) = \int_0^\infty f_{u,\dot{u}}(u_\tau, w)\,w\,dw$, the LCR at the output of the SOA yields

$$\mathrm{LCR}\,(u_\tau) = \sqrt{\frac{2}{\pi}}\,\frac{m_y^{m_y}\,m_x^{m_x}}{\Gamma(m_y)\,\Gamma(m_x)}\left[\frac{1}{r}\,\log\left[\mathcal{T}(r\,u_\tau)\right]\right]^{m_y-\frac{1}{2}}$$

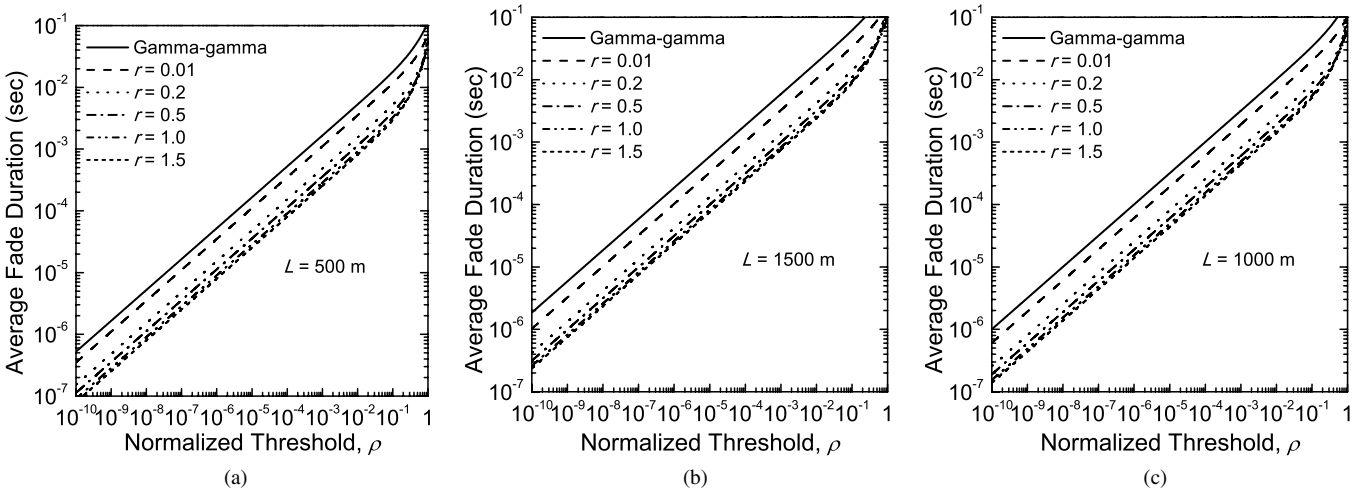

Fig. 7. Average fade duration at the output of the SOA versus the normalized threshold ρ for $G_0 = 20$ dB and $L = 0.5$, 1.0 and 1.5 km. (a) $L = 0.5$ km. (b) $L = 1.0$ km. (c) $L = 1.5$ km.

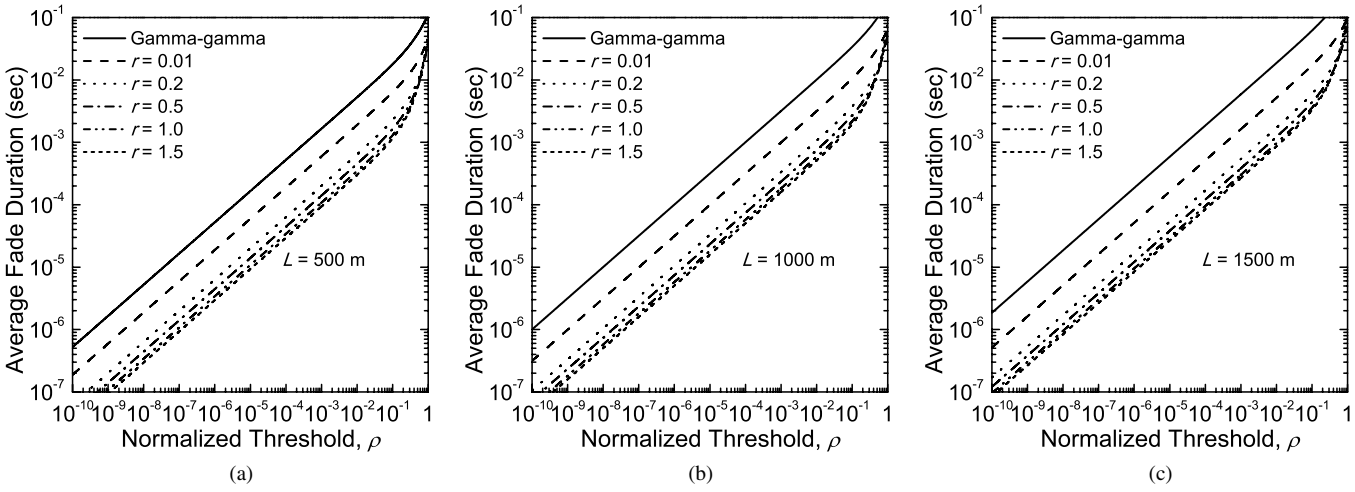

Fig. 8. Average fade duration at the output of the SOA versus the normalized threshold ρ for $G_0 = 30$ dB and $L = 0.5$, 1.0 and 1.5 km. (a) $L = 0.5$ km. (b) $L = 1.0$ km. (c) $L = 1.5$ km.

$$\times \int_0^\infty q^{m_x - m_y - \frac{3}{2}} \exp(-m_x q)[\log[\mathcal{T}(r u_\tau)]]^{-\frac{m_y}{r,q}}$$

$$\times \sqrt{\frac{b_x^2}{r}\, \log\left[\mathcal{T}(r\, u_\tau)\right] + b_y^2\, q^2}\, dq \tag{25}$$

while the AFD is finally derived using (16) and (25) as

$$\mathrm{AFD}\,(u_\tau) = \frac{\Pr\{u < u_\tau\}}{\mathrm{LCR}\,(u_\tau)}. \tag{26}$$

Equation (26) is plotted in Figs. 7 and 8 against the normalized threshold ρ for the $\gamma - \gamma$ parameters of Tables I and II. The figure illustrates that the AFD reduction that can be attained by the SOA is very similar for all link lengths, and is approximately equal to 85% for the 20 dB gain device and 95% for its 30 dB counterpart. As a result, the duration of fades and therefore the system latency can be decreased by more than one order of magnitude by utilizing the SGM-based SOA equalizer, provided that the SOA is saturated to the appropriate level. Similarly to the results that have been obtained for the first order statistics, a signal power of approximately 50% of the SOA saturation parameter is adequate to attain practically maximum AFD reduction.

V. Conclusion and Future Work

We have proposed and theoretically investigated a fade mitigation technique based on SGM in SOAs. We have analytically demonstrated that the power equalization properties of the SOA are adequate to alter the ill-behaved $\gamma - \gamma$ statistics of the incoming OW signal and provide an output signal that exhibits less intense and shorter-lived fluctuations. To this end, we derived the first and second order statistics of the OW signal at the SOA output and showed that the probability and duration of fades are drastically decreased. Even though this work was limited to $\gamma - \gamma$ fading statistics, the presented methodology can be also applied to obtain results for weak (log-normal statistics) and very intense fading (exponential statistics), whose individual and joint pdfs have been also well-studied.

It should be noted that the presented analysis is based on the following important assumptions: a) the SOA gain can fully

recover between pulses, b) the system is not impaired by optical noise, and c) the received optical power is sufficient to saturate the SOA. The first assumption is valid for contemporary OW links that operate at 10 Gb/s, since commercially available SOAs exhibit gain recovery times of less than 100 psec and can support the aforementioned line rates. Future endeavors that will assess fade equalization in SOAs at higher rates will require more accurate SOA models that call for a numerical evaluation of the SOA gain temporal profile [26], or will even lead to the replacement of the SGM equalizer by higher capacity optical signal processing arrangements that rely on SOA-based interferometers [27] or filtering setups [28], [29], which exhibit recovery times of less than 10 ps.

With respect to noise, two major noise contributions are expected: background noise and amplified spontaneous emission (ASE) in the SOA. Background (solar) noise does not exhibit significant power levels at 1550 nm [30], still it is amplified in the SOA and aggravates the system optical signal-to-noise-ratio (OSNR) at the presence of fades. In a similar fashion, ASE contributes to the creation of noise-signal and noise-noise beating terms at the receiver [31], and corrupts the equalization process due to the compression of the available gain. A detailed analysis of the ASE noise impact on the operation of the proposed equalizer is beyond the scope of this study, but we expect that the equalized system performance will be better than that of the non-equalized one even at the presence of ASE noise. This can be established by taking into consideration that the amplification process lowers the receiver sensitivity and allows for more intense power fluctuations despite the OSNR degradation during fades [32]. The sensitivity improvement is not taken into account in the presented analysis, but will add to the predicted scintillation improvement and will result in even lower fade probabilities than those demonstrated. Furthermore, the impact of noise can be reduced if continuous wave (CW)-assisted optical regeneration and/or noise reduction techniques are considered to supress the available gain in the SOA, and therefore the ASE noise power at its output. This principle is not directly applicable to the proposed SGM equalizer, since our results demonstrate that the equalizer performance is better at high gains, but it can be applied at the aforementioned interferometric and filtering setups at the added benefit of a faster response.

Finally, driving the SOA at the input power levels that are suggested by our analysis for optimal operation can be challenging from a practical perspective, given that its saturation energy equals to a few pJ and results in a saturation parameter of tens of mW at 10 Gb/s. Due to the increased losses of OW communication systems, which can amount to 20 dB/km or more, an additional amplification stage may be required prior to the SOA to provide the input powers in the order of mW. The impact of the pre-amplifier on the signal quality can be rather limited provided that it is designed as a high-gain and low-noise element. Alternatively, the SOA can be operated at lower optical powers and, despite the fact that this mode of operation does not realize the full potential of the proposed technique, the equalized system will still exhibit improved fade probabilities and durations than the non-equalized one. Yet another option is to utilize interferometric and filter-assisted equalizers that take advantage of CW gain saturation to lower the input energy requirements. Previously reported works on similar setups have demonstrated successful operation at pulse energies as low as a few tens of fJ [29], [33].

APPENDIX

GAMMA-GAMMA CHANNEL MODEL PARAMETERS

For a plane wave with a zero inner scale and an infinite outer scale of turbulence, the $\gamma-\gamma$ parameters m_x and m_y are given by [22]

$$m_x = \frac{1}{\exp\left(\sigma^2_{\ln x}\right) - 1} \tag{A-1a}$$

and

$$m_y = \frac{1}{\exp\left(\sigma^2_{\ln y}\right) - 1} \tag{A-1b}$$

respectively. The log-intensity variances are given by

$$\sigma^2_{\ln x} = 0.16\,\sigma_R^2\,\left(\frac{\eta_x}{1 + 0.25\,d^2\,\eta_x}\right)^{7/6} \tag{A-2a}$$

and

$$\sigma^2_{\ln y} = 1.27\,\sigma_R^2\,\frac{\eta_y^{-5/6}}{1 + 0.3\,d^2\,\eta_y} \tag{A-2b}$$

where

$$\eta_x = \frac{2.61}{1 + 1.11\,\sigma_R^{12/5}} \tag{A-3a}$$

and

$$\eta_y = 3\,\left(1 + 0.69\,\sigma_R^{12/5}\right). \tag{A-3b}$$

Parameter d corresponds to the receiver aperture radius normalized by the Fresnel zone

$$d = \sqrt{\frac{k\,D^2}{4\,L}} \tag{A-4}$$

with k being the wave-number and L being the link length. σ_R^2 denotes the Rytov variance

$$\sigma_R^2 = 1.23\,C_n^2\,k^{7/6}\,L^{11/6} \tag{A-5}$$

with C_n^2 being the refractive index structure parameter.

Parameters b_x and b_y in the second order statistics of the $\gamma-\gamma$ channel model are calculated by

$$b_x^2 = \frac{1.06\,k\,v_T^2}{8\,L}\,\sigma_R^2\int_0^1\int_0^\infty \eta^{-5/6}\,\exp\left(-\frac{\eta\,d^2}{4} - \frac{\eta}{\eta_x}\right) \times\left[1 - \cos\left(\eta\,\xi\right)\right]\,d\eta\,d\xi \tag{A-6a}$$

and

$$b_y^2 = \frac{1.06\,k\,v_T^2}{8\,L}\,\sigma_R^2\int_0^1\int_0^\infty (\eta+\eta_y)^{-11/6}\,\exp\left(-\frac{\eta\,d^2}{4}\right) \times\,\eta\,\left[1 - \cos\left(\eta\,\xi\right)\right]\,d\eta\,d\xi \tag{A-6b}$$

with v_T representing the mean transverse wind speed.

REFERENCES

[1] Q. Liu, C. Qiao, G. Mitchell, and S. Stanton, "Optical wireless communication networks for first- and last-mile broadband access," *OSA J. Opt. Netw.*, vol. 4, no. 12, pp. 807–828, Dec. 2005.

[2] R. S. Lawrence and J. W. Strohbehn, "A survey of clear-air propagation effects relevant to optical communications," *Proc. IEEE*, vol. 58, no. 10, pp. 1523–1545, Oct. 1970.
[3] L. C. Andrews and R. L. Phillips, *Laser Beam Propagation Through Random Media*, 2nd ed. Bellingham, WA, USA: SPIE Press, 2005.
[4] V. W. S. Chan, "Free-space optical communications," *J. Lightw. Technol.*, vol. 24, no. 12, pp. 4750–4762, Dec. 2006.
[5] H. Yuksel, S. Milner, and C. C. Davis, "Aperture averaging for optimizing receiver design and system performance on free-space optical communication links," *OSA J. Opt. Netw.*, vol. 4, no. 8, pp. 462–475, Jul. 2005.
[6] S. G. Wilson, M. Brandt-Pearce, Q. Cao, and M. Baedke, "Optical repetition MIMO transmission with multi-pulse PPM," *IEEE J. Sel. Areas Commun.*, vol. 23, no. 9, pp. 1901–1910, Sep. 2005.
[7] S. M. Navidpour, M. Uysal, and M. Kavehrad, "BER performance of free-space optical transmission with spatial diversity," *IEEE Trans. Wireless Commun.*, vol. 6, no. 8, pp. 2813–2819, Aug. 2007.
[8] A. Goldsmith, S. A. Jafar, N. Jindal, and S. Vishwanath, "Capacity limits of MIMO channels," *IEEE J. Sel. Areas Commun.*, vol. 21, no. 5, pp. 684–702, Jun. 2003.
[9] M.-A. Khalighi, N. Schwartz, N. Aitamer, and S. Bourennane, "Fading reduction by aperture averaging and spatial diversity in optical wireless systems," *IEEE/OSA J. Opt. Netw.*, vol. 1, no. 6, pp. 580–593, Nov. 2009.
[10] A. García-Zambrana, C. Castillo-Vázquez, and B. Castillo-Vázquez, "Outage performance of MIMO FSO links over strong turbulence and misalignment fading channels," *OSA Opt. Exp.*, vol. 19, no. 14, pp. 13480–13496, Jun. 2011.
[11] S. Trisno, I. I. Smolyaninov, S. D. Milner, and C. C. Davis, "Delayed diversity for fade resistance in optical wireless communication system through simulated turbulence," in *Optical Transmission Systems and Equipment for WDM Networking III*. vol. 5596, Philadelphia, PA, USA: SPIE, Oct. 2004, pp. 385–393.
[12] J. A. Greco, "Design of the high-speed framing, FEC, and interleaving hardware used in a 5.4 km free-space optical communication experiment," in *Free-Space Laser Communications IX*. vol. 7464, San Diego, CA, USA: SPIE, Aug. 2009.
[13] X. Zhu and J. M. Kahn, "Performance bounds for coded free-space optical communications through atmospheric turbulence channels," *IEEE Trans. Commun.*, vol. 51, no. 8, pp. 1233–1239, Aug. 2003.
[14] I. B. Djordjevic, "LDPC-coded MIMO optical communication over the atmospheric turbulence channel using Q-ary pulse-position modulation," *OSA Opt. Exp.*, vol. 15, no. 16, pp. 10026–10032, Jun. 2007.
[15] H. Henniger, F. David, D. Giggenbach, and C. Rapp, "Evaluation of FEC for the atmospheric optical IM/DD channel," in *Free-Space Laser Communication Technologies XV*. vol. 4975, San Jose, CA, USA: SPIE, Jul. 2003.
[16] A. Anguita, M. A. Neifeld, B. Hildner, and B. Vasic, "Rateless coding on experimental temporally correlated FSO channels," *J. Lightw. Technol.*, vol. 28, no. 7, pp. 990–1002, Apr. 2010.
[17] M. Abtahi, P. Lemieux, W. Mathlouthi, and L. A. Rusch, "Suppression of turbulence-induced scintillation in free-space optical communication systems using saturated optical amplifiers," *J. Lightw. Technol.*, vol. 24, no. 12, pp. 4966–4973, Dec. 2006.
[18] G. P. Agrawal and N. A. Olsson, "Self-phase modulation and spectral broadening of optical pulses in semiconductor laser amplifiers," *IEEE J. Quantum Electron.*, vol. 25, no. 1, pp. 2297–2306, Nov. 1989.
[19] M. Eiselt, W. Pieper, and H. G. Weber, "SLALOM: Semiconductor laser amplifier in a loop mirror," *J. Lightw. Technol.*, vol. 19, no. 10, pp. 2099–2112, Oct. 1995.
[20] M. A. Al-Habash, R. L. Phillips, and L. C. Andrews, "Mathematical model for the irradiance probability density function of a laser beam propagating through turbulent media," *Opt. Eng.*, vol. 40, no. 8, pp. 1554–1562, Aug. 2001.
[21] P. S. Bithas, N. C. Sagias, P. T. Mathiopoulos, G. K. Karagiannidis, and A. A. Rontogiannis, "On the performance analysis of digital communications over generalized-K fading channels," *IEEE Commun. Lett.*, vol. 10, no. 5, pp. 353–355, May 2006.
[22] L. C. Andrews, R. L. Phillips, and C. Y. Hopen, *Laser Beam Scintillation with Applications*. Bellingham, WA, USA: SPIE Press, 2001.
[23] F. S. Vetelino, C. Young, L. C. Andrews, and J. Recolons, "Aperture averaging effects on the probability density of irradiance fluctuations in moderate-to-strong turbulence," *Appl. Opt.*, vol. 46, no. 11, pp. 2099–2108, Apr. 2007.
[24] M. K. Simon and M.-S. Alouini, *Digital Communication over Fading Channels*, 2nd ed. New York, NY, USA: Wiley, 2005.
[25] F. S. Vetelino, "Fade statistics for a lasercom system and the joint pdf of a gamma-gamma distributed irradiance and its time derivative" Doctoral dissertation, Univ. Central Florida, Orlando, FL, USA, Jan. 2006.
[26] A. Mecozzi and J. Mørk, "Saturation induced by picosecond pulses in semiconductor optical amplifiers," *J. Opt. Soc. Amer. B*, vol. 14, no. 4, pp. 761–770, Apr. 1997.
[27] K. Tajima, "All-optical switch with switch-off time unrestricted by carrier lifetime," *Jpn. J. Appl. Phys.*, vol. 32, no. 12A, pp. L1746–L1749, Dec. 1993.
[28] Y. Lianshan, A. E. Willner, W. Xiaoxia, Y. Anlin, A. Bogoni, Z.-Y. Chen, and H.-Y. Jiang, "All-optical signal processing for ultrahigh speed optical systems and networks," *J. Lightw. Technol.*, vol. 30, no. 24, pp. 3760–3770, Dec. 2012.
[29] Y. Liu, E. Tangdiongga, Z. Li, S. Zhang, H. de Waardt, G.-D. Khoe, and H. J. S. Dorren, "Error-free all-optical wavelength conversion at 160 Gb/s using a semiconductor optical amplifier and an optical bandpass filter," *J. Lightw. Technol.*, vol. 24, no. 1, pp. 230–236, Jan. 2006.
[30] D. K. Borah, A. C. Boucouvalas, C. C. Davis, S. Hranilovic, and K. Yiannopoulos, "A review of communication-oriented optical wireless systems," *EURASIP J. Wireless Commun. Netw.*, vol. 91, pp. 1–28, Apr. 2012.
[31] N. A. Olsson, "Lightwave systems with optical amplifiers," *J. Lightw. Technol.*, vol. 7, no. 7, pp. 1071–1082, Jul. 1989.
[32] R. Ramaswami, K. N. Sivarajan, and G. Sasaki, *Optical Networks: A Practical Perspective*, 3rd ed. San Francisco, CA, USA: Morgan Kaufmann, Jul. 2009.
[33] N. Pleros, C. Bintjas, G. T. Kanellos, K. Vlachos, H. Avramopoulos, and G. Guekos, "Recipe for intensity modulation reduction in SOA-based interferometric switches," *J. Lightw. Technol.*, vol. 22, no. 12, pp. 2834–2841, Dec. 2004.

Konstantinos Yiannopoulos (S'03–M'05) received the Diploma and Ph.D. degrees in electrical and computer engineering in 2000 and 2004, respectively, from the School of Electrical and Computer Engineering, National Technical University of Athens, Athens, Greece.

He is a Lecturer at the University of Peloponnese, Greece. He was a member of the research teams of the Photonics Communications Research Laboratory at the National Technical University of Athens, Greece, from 2000 to 2004, and the Computer Networks Laboratory at the University of Patras, Greece, from 2005 to 2010. During this period, he conducted a research on physical layer (optical signal processing, ultrafast optical sources, all-optical logic) and network layer (optical packet and burst switching networks) aspects of optical networks. At the present time, he is conducting a research that focuses on optical wireless networks (system architectures and protocol analysis).

Dr. Yiannopoulos has more than 40 published papers in international journals and conferences. His research work was granted with the "IEEE/LEOS Graduate Student Fellowship Program 2004" award and has received more than 300 independent citations.

Nikos C. Sagias (S'03–M'05–SM'11) was born in Athens, Greece, in 1974. He received the B.Sc. degree from the Department of Physics (DoP), the University of Athens (UoA), Athens, Greece, in 1998. He received the M.Sc. and Ph.D. degrees in telecommunication engineering from the UoA in 2000 and 2005, respectively. Since 2001, he has been involved in various National and European Research & Development projects for the Institute of Space Applications and Remote Sensing of the National Observatory of Athens, Greece. During 2006–2008, he was a Research Associate at the Institute of Informatics and Telecommunications of the National Centre for Scientific Research-"Demokritos," Athens, Greece. Currently, he is an Assistant Professor at the Department of Informatics and Telecommunications of the University of Peloponnese, Tripoli, Greece. His research interests include wireless digital communications, and more specifically MIMO and cooperative diversity systems, fading channels, and communication theory. Dr. Sagias In his record, he has more than 40 papers in prestigious international journals and more than 30 in the proceedings of world recognized conferences. He is an Editor for the IEEE TRANSACTIONS ON WIRELESS COMMUNICATIONS, while he acts as a TPC member for various IEEE conferences (GLOBECOM, VTC, WCNC, etc.). He is a corecipient of the Best Paper Award in communications in the 3rd International Symposium on Communications, Control and Signal Processing, Malta, March 2008. He is a member of the IEEE Communications Society as well as the Hellenic Physicists Association.

Anthony C. Boucouvalas (M'81–SM'00–F'02) received the B.Sc. degree in electrical and electronic engineering from Newcastle upon Tyne University, U.K., in 1978. He received the M.Sc. and D.I.C. degrees in communications engineering, in 1979 and in 1982, respectively, and the Ph.D. degree in fibre optics, all from Imperial College, London, U.K.

He is a Professor in Communication Networks and Applications at the University of Peloponnese in Tripoli, Greece. He has been actively involved with research in various aspects of fiber-optic communications, wireless communications, and multimedia, and has an accumulated 25 years working experience in well-known academic and industrial research centers. He was a Professor in Multimedia Communications and Director of the Microelectronics and Multimedia Communications Research Centre of Bournemouth University until 2006. From 1987 to 1994, he has worked as a Project Manager for Hewlett Packard Laboratories and was involved with many projects in the fields of optical communications, optical networks, and optical instrumentation. In 1982, he worked as a Group Leader and Divisional Chief Scientist at GEC Hirst Research Laboratories in the fields of fiber-optic components, measurements, and sensors.

Prof. Boucouvalas' research spans a wide range of topics in communications and multimedia, both from the theoretical as well as the practical points of view. His recent work has been directed toward communication protocol problems arising from various areas of wireless communication, expressive internet communications, effective human–computer interfaces and inverse fiber-optic problems. His work has been supported by numerous research grants and contracts from European Union and industrial organizations, and has been published in over 260 publications. He is a Fellow of the Institution of Electrical Engineers and of the IEEE. He has also been a member of the Architectures Council of the Infrared Data Association since 2003.